Journal of Electroanalytical Chemistry 736 (2015) 127–131

Contents lists available at ScienceDirect

Journal of Electroanalytical Chemistry

journal homepage: www.elsevier.com/locate/jelechem

# S–$TiO_2$ composite cathode materials for lithium/sulfur batteries

Xin Zhou Ma, Bo Jin *, Hui Yuan Wang *, Jia Zi Hou, Xiao Bin Zhong, Huan Huan Wang, Pei Ming Xin

*Key Laboratory of Automobile Materials, Ministry of Education, College of Materials Science and Engineering, Jilin University, Changchun 130025, China*

ARTICLE INFO

*Article history:*
Received 23 July 2014
Received in revised form 3 November 2014
Accepted 6 November 2014
Available online 15 November 2014

*Keywords:*
S–$TiO_2$ composite
Cathode materials
Lithium/sulfur batteries

ABSTRACT

$TiO_2$ nanofibers were prepared by improved electrospinning technique and subsequent thermal treatment. The as-prepared $TiO_2$ nanofibers possess anatase-rutile mischcrystal structure. Sulfur was mixed with the $TiO_2$ nanofibers to form S–$TiO_2$ composite by a melt diffusion process. The S–$TiO_2$ composite displays more excellent discharge capacity retention of 58% after 50 cycles compared to pure S, and the discharge capacity is 530 mAh $g^{-1}$ after 50 cycles, which is ascribed to the adsorption of lithium polysulfide by $TiO_2$.



## 1. Introduction

Recently, high-specific-energy rechargeable lithium-ion batteries (LIBs) and sodium-ion batteries have attracted ever-increasing attention due to the increasing energy demands and environmental crisis [1–3]. However, the current insertion oxide cathodes such as $LiCoO_2$ and $LiMn_2O_4$ with low capacity (<300 mAh $g^{-1}$) have limited the performance of LIBs, which forces material researchers to develop alternative high-capacity cathodes [4–6]. In the new cathode materials, sulfur is very attractive for LIBs due to its high theoretical specific capacity of 1675 mAh $g^{-1}$, which is about five times higher than the current insertion oxide cathodes. In addition, sulfur is abundant, low-cost, non-toxic and environmental friendly [7–13]. Therefore, lithium/sulfur batteries have the potential to replace current LIBs in the near future [11,12].

However, there are many challenges remained for lithium/sulfur batteries before the commercialized application, that is as follows: (i) electric insulating of sulfur and the insoluble low-order lithium polysulfide; (ii) high dissolution of intermediate polysulfides, creating an internal "shuttle" phenomenon which causes an irreversible loss of sulfur and low coulombic efficiency; and (iii) large volumetric expansion of sulfur (80%) during the discharge/charge process [14–18]. To solve the above problems, extensive attempts have been made, including the use of various carbon [19–22] or conductive polymer substrates [23–27], the optimization of organic electrolyte [28–32] and the utilization of porous oxide additives [33–35]. Zheng et al. [32] utilized ionic liquid (IL) *N*-methyl-*N*-butylpyrrolidinium bis(trifluoromethylsulfonyl)imide to modify the properties of the SEI layer formed on the Li metal surface in Li–S batteries. It was found that the IL-enhanced passivation film on the lithium anode surface exhibited very different morphology and chemical composition, effectively protecting lithium metal from continuous attack by soluble polysulfides. Recently, $TiO_2$ as an additive or a substrate [14,16,36–39] for lithium/sulfur batteries has received much attention because its strong chemical adsorption of lithium polysulfide, which can significantly improve the cycle performance of lithium/sulfur batteries. Seh et al. [14] fabricated sulfur-$TiO_2$ (amorphous) yolk-shell nanoarchitecture with an internal void space, which displayed a long cycling capability (over 1000 charge/discharge cycles) with a small decay rate of 0.033% per cycle. Li et al. [39] designed a sulfur-impregnated mesoporous hollow $TiO_2$ (anatase) sphere cathode with intriguing capacity retention (71%) and high coulombic efficiency (93%) over 100 cycles at 1 C rate. To our knowledge, there is no paper related to $TiO_2$ with anatase-rutile mischcrystal structure as the improved matrix for lithium/sulfur batteries.

In this paper, $TiO_2$ nanofibers were prepared by improved electrospinning technique and subsequent thermal treatment. Electrospinning can offer a simple and versatile route to the large-scale production of fibers from a variety of materials [40]. Sulfur was mixed with the $TiO_2$ nanofibers to form S–$TiO_2$ composite by a melt diffusion process. The structural and morphological performance of the S–$TiO_2$ composite was investigated by X-ray diffraction, transmission electron microscopy, scanning electron microcopy and field emission scanning electron microscopy, and the electrochemical properties were analyzed by cyclic voltammograms and galvanostatic discharge/charge tests.

* Corresponding authors. Tel.: +86 431 85095170.
*E-mail addresses:* jinbo@jlu.edu.cn (B. Jin), wanghuiyuan@jlu.edu.cn (H.Y. Wang).

http://dx.doi.org/10.1016/j.jelechem.2014.11.007
1572-6657/

## 2. Experimental

### 2.1. Materials synthesis

$TiO_2$ nanofibers were prepared by improved electrospinning technique and subsequent thermal treatment as described by the previous reports [40,41]. In a typical synthesis, 0.35 g poly (vinyl pyrrolidone) was added to a mixture of 6.5 mL ethanol, 2 mL acetic acid and 1.5 mL tetrabutyl titanate, and then stirred for 10 h at room temperature in order to obtain a homogeneous precursor solution. The solution was driven from the syringe by a syringe pump (ALC-IP900, Shanghai Alcott Biotech. Co., Ltd.) at a constant rate of 1 mL $h^{-1}$. $TiO_2$ nanofibers were electrospun at 20 kV using a high voltage power supply (Tianjin Dongwen High Voltage Facility) with a 10 cm collection distance. $TiO_2$ nanofibers were collected on a grounded aluminum (Al) foil collector and left overnight in air to fully hydrolyze, and then calcined in air at 500 °C for 6 h.

As-prepared $TiO_2$ nanofibers were ground for 15 min, and then mixed with sulfur at a weight ratio of 40:60. The mixture was ball-milled for 2 h at 200 rpm in ethanol. The obtained mixture was dried at 60 °C for 12 h to remove the solvent, and then heated to 155 °C for 12 h in a sealed 50 mL Teflon-lined stainless-steel autoclave. After cooling down to room temperature, the S–$TiO_2$ composite was obtained. The synthesis route for the S–$TiO_2$ composite is illustrated in Fig. 1.

### 2.2. Material characterization

The synthesized products were characterized by powder X-ray diffraction (XRD, Dmax/2500PC, Rigaku, Japan) with Cu Kα radiation ($\lambda$ = 1.5406 Å), scanning electron microscopy (SEM, ZEISS EVO 18, Germany), field emission scanning electron microscopy (FESEM, JSM-6700F, Japan) and high-resolution transmission electron microscopy (HRTEM, FEI Tecnai G2 F20, operating at an accelerating voltage of 200 kV, USA). The elements on the surface of S–$TiO_2$ were identified by energy-dispersive X-ray spectroscopy. The $N_2$ adsorption/desorption tests were determined by Brunauer–Emmett–Teller (BET) measurements using an NOVA1000 surface area analyzer. Thermogravimetric analysis (TGA) was carried out to determine the weight content of sulfur in the composite at a heating rate of 10 °C $min^{-1}$ under $N_2$ atmosphere.

### 2.3. Electrochemical measurements

The electrochemical tests were conducted by assembling coin-type batteries (CR2025) in an argon-filled glove box and lithium metal was used as both counter and reference electrode. The working electrodes were prepared by a slurry coating procedure. The slurry was made by mixing 70 wt% S–$TiO_2$ composite, 20 wt% acetylene black and 10 wt% polyvinylidene fluoride in *N*-methyl-2-pyrrolidinone solvent. The slurry was uniformly spread onto Al foil and dried at 60 °C for 12 h in a vacuum oven. The used electrolyte was 1 M $LiCF_3SO_3$ in a mixed solvent of dimethoxyethane and dioxolane with a volume ratio of 50:50 containing 0.1 M $LiNO_3$ as an electrolyte additive. The discharge and charge performance of half-cells was tested with LAND CT-2001A battery instrument at a current density of 335 mA $g^{-1}$ in the voltage range of 1.5–3.0 V at ambient temperature, and rate performance was also tested at different current densities in the same voltage range. The specific capacity was calculated on the basis of the active sulfur material. Pure sulfur cathode was also prepared in the same way just in the absence of $TiO_2$ to compare with the S–$TiO_2$ composite. Pure $TiO_2$ cathode was also prepared in the same way to indicate its role in the S–$TiO_2$ composite. Cyclic voltammogram (CV) measurements were carried out on an electrochemical workstation (CHI650D, Shanghai Chenhua Instruments Ltd.) at a scan rate of 0.1 mV $s^{-1}$ from 1.5 to 3.0 V at room temperature.

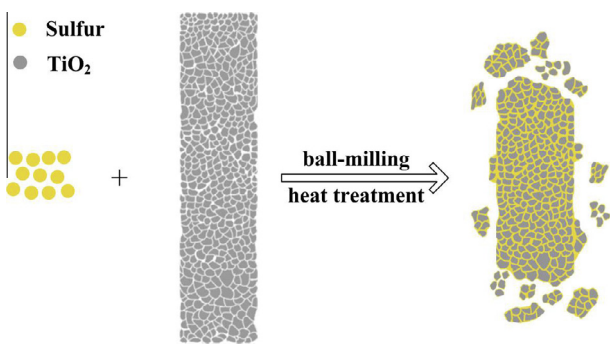


**Fig. 1.** The synthesis schematic diagram of S–$TiO_2$.

## 3. Results and discussion

XRD patterns of pure S, $TiO_2$ and S–$TiO_2$ are shown in Fig. 2. As shown in Fig. 2(a), all patterns of pure S can be indexed to a material having an orthorhombic structure, which is in good agreement with the one listed in the X-ray powder diffraction data file (JCPDS No. 24-0733) by the American Society for Testing Materials as standard. Fig. 2(c) demonstrates that $TiO_2$ possesses anatase (JCPDS No. 01-0562)-rutile (JCPDS No. 65-0191) mischcrystal structure. As for S–$TiO_2$, there are no any new phases in the final product except pure S and anatase-rutile mischcrystal, which could be an indication of the absence of chemical reaction between the composite components upon ball milling and the following heat treatment [38,42], only peak densities decrease compared to those of pure S and anatase-rutile mischcrystal, indicating the good dispersion of sulfur in the S–$TiO_2$ composite [37]. It is obvious that the added anatase-rutile mischcrystal does not change the crystal structure of pure S.

TGA curve of S–$TiO_2$ under $N_2$ atmosphere is shown in Fig. 3. As can be seen in Fig. 3, a weight loss of 57.5 wt% is found between 200 and 300 °C corresponding to the evaporation of sulfur. Therefore, the sulfur content is determined to be 57.5 wt% in the S–$TiO_2$ composite.

SEM image of pure S and FESEM images of $TiO_2$ and S–$TiO_2$ are shown in Fig. 4. TEM image of S–$TiO_2$ and FESEM image of S–$TiO_2$ and the corresponding element mapping of Ti and S is also displayed in Fig. 4. Pore size distribution curves and the specific surface areas of pure S and S–$TiO_2$ are shown in Fig. 5. As shown in Fig. 4(a), the particle size of pure S is around 10–50 μm and in

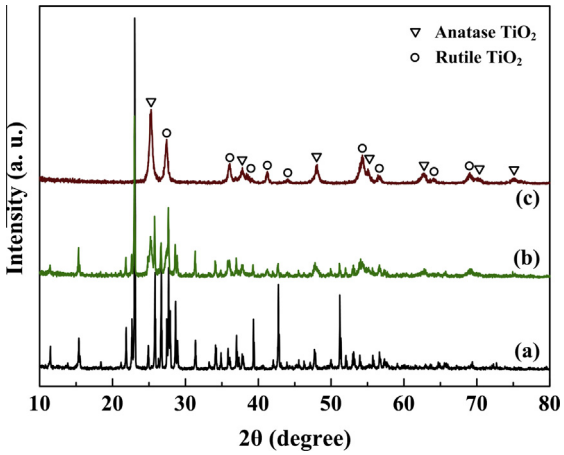


**Fig. 2.** XRD patterns of (a) Pure S, (b) S–$TiO_2$ and (c) $TiO_2$.